*International Journal of Rotating Machinery*
2001, Vol. 7, No. 3, pp. 209–222
Reprints available directly from the publisher
Photocopying permitted by license only



# Numerical Computation of Turbulent Flow and Heat Transfer in a Radially Rotating Channel with Wall Conduction*

FRANK K. T. LIN[a], G. J. HWANG[a], S.-C. WONG[a] and C. Y. SOONG[b,†]

[a]*Department of Power Mechanical Engineering, National Tsing Hua University, Hsinchu, Taiwan 30043, ROC;* [b]*Rotating Fluids and Vortex Dynamics Laboratory, Department of Aeronautical Engineering, Chung Cheng Institute of Technology, Tahsi, Taoyuan, Taiwan 33509, ROC*

*(Received 8 July 2000; In final form 13 July 2000)*

This work is concerned with numerical computation of turbulent flow and heat transfer in experimental models of a radially rotating channel used for turbine blade cooling. Reynolds-averaged Navier–Stokes and energy equations with a two-layer turbulence model are employed as the computational model of the flow and temperature fields. The computations are carried out by the software package of "CFX-TASCflow". Heat loss from the channel walls through heat conduction is considered. Results at various rotational conditions are obtained and compared with the baseline stationary cases. The influences of the channel rotation, through-flow, wall conduction and the channel extension on flow and heat transfer characteristics are explored. Comparisons of the present predictions and available experimental data are also presented.

*Keywords*: Rotating channel; Turbulence model; Wall conduction; Turbine blade cooling

## INTRODUCTION

Advanced gas turbine engines require high thermal efficiency and high power density. Therefore, turbine blades must be cooled in order to operate in an environment of high gas temperature and to extend their durability. Many cooling techniques have been proposed over the years, among those the forced convection internal cooling is one of the most important ones. The flow and heat transfer characteristics inside a rotating heated channel are very complicated. They are not only affected by the main flow but also influenced by the Coriolis-induced cross-stream and centrifugal buoyancy effect in longitudinal direction. Due to different rotational effects on the flows in near-wall regions,

*The original version of this paper was presented at ISROMAC-8.

†Corresponding author. e-mail: cysoong@ccit.edu.tw

the heat transfer performance on the four walls, *i.e.*, leading wall (suction side), trailing wall (pressure side), and two side-walls, may differ from each other. This rotational effect will alter the turbulence characteristics in the channel flows either.

In the literature, a number of experimental studies have been conducted to understand the fundamental heat transfer and fluid flow phenomena in radially rotating passages. Johnston *et al.* (1972) investigated the effect of Coriolis force on the structure of turbulence in a radially rotating channel. When the rotation number increases, turbulent mixing is enhanced on the trailing wall and diminished on the leading wall. Abdelmeguid and Spalding (1979) found that the buoyancy forces tend to reduce the laminar heat transfer rate but enhance the turbulent heat transfer rate for a radially outward flow. Morris and Ghavami-Nasr (1991) conducted heat transfer measurements in rectangular channels with orthogonal mode rotation and showed that the Coriolis-induced secondary flow enhances local heat transfer on the trailing wall and the converse is true on the leading wall where significant impediment to local heat transfer can occur. Soong *et al.* (1991) revealed that the overall heat transfer rate is enhanced by the Coriolis force but degraded by the centrifugal buoyancy. In rotating passages with smooth walls and radial outward flow, Wagner *et al.* (1991) found that heat transfer rate becomes 3.5 times on the trailing wall and decreases 40% on the leading wall. Han and Zhang (1992) studied the effect of uneven wall temperature on local heat transfer in a rotating square channel with smooth walls and radially outward flow. The results showed that the local heat transfer coefficients on the leading, trailing, and side-walls are altered by the uneven wall temperature. Kuo and Hwang (1996) measured local heat transfer distributions in a uniformly heated rotating square duct, and addressed the influences of the rotational effects. Most recently, Hwang *et al.* (1999) studied the heat transfer of compressed air flow in a rotating four-pass serpentine channel at $Re = 20000$, 30000 and 40000, and rotating rates ranging from 0 to 1250 rpm. Details of the local heat transfer along the four-pass channel were addressed.

As to the numerical simulation, more difficulties can be expected for the complexities of the physics and the uncertainties of the numerical procedure and the modeling. Iacovides and Launder (1987, 1991) used standard $k-\varepsilon$ eddy-viscosity and algebraic second-moment closure turbulence models to predict the flow field and heat transfer in a square ducts rotating in orthogonal mode. Low rotating rates cause the formation of a pair of symmetric streamwise vortices. While the flow instabilities on the pressure side lead the two-vortex flow pattern to a four-vortex structure at higher rotating rates. Iacovides and Launder (1995) gave some comments in their review paper of CFD applications to internal cooling of gas-turbine blade. One of them is the use of a two-equation linear eddy-viscosity model in the turbulent core coupled with a simple one-equation model across the sublayer. It provides a useful route for tackling most of the flows considered. Although it may not achieve prediction of highest quality, it is a straightforward level of modeling to use and has a good track for capturing the broad trends. Dutta *et al.* (1996) employed the modeled turbulence generation terms for the Coriolis and buoyancy effects in the $k-\varepsilon$ transport equations and obtained a better agreement with the experimental data.

In the past, most previous computational models used in numerical simulation did not include the effects of wall conduction and the channel extension attached at the inlet and/or outlet of the experimental model. To explore these influences on the computational results of heat transfer performance, a typical geometry of the experimental model used in Kuo and Hwang (1996) is considered. The thickness of the duct wall and the heat loss from the outer surface is included in the present numerical work. Also, some computations include the channel extensions attached at the two ends of the model.

## PROBLEM STATEMENT

### Description of Physical Models

Figure 1 shows the description of the physical model and the coordinate system. The square channel is composed of inner flow passage and outer wall region. Two models are considered in the simulation. One model has no extended part at two ends of the test duct. The axial length, height and width of the heating duct are 0.12, 0.004 and 0.004 m, respectively. The hydraulic diameter ($D$) of the flow passage is 0.004 m. The outer supporting part of the duct is formed by fiberglass of 0.003 m in thickness. The inner surfaces of the walls are stainless steel film of thickness 0.01 mm, which are also used as electric film heaters. A constant heat source is applied to the heaters. The channel length, heater actively heating length, and the mean rotational radius are 0.12, 0.12 and 0.18 m, respectively. Another model has two extensions of 0.1 m ($25D$) and 0.04 m ($10D$) length attached at the inlet and the outlet, respectively. The total length of this model becomes 0.26 m. The cross-sectional views of the models are shown in Figures 1(b) and 1(c).

### Governing Equations

Computations are performed for numerical solution of the three-dimensional Reynolds-averaged Navier–Stokes, energy equations and $k-\varepsilon$ equations, which can be found elsewhere and are not listed herein. In this study, a two-layer turbulence model is used. In the central region of the duct, the standard $k-\varepsilon$ model is employed; while in the near-wall region, one equation model is used to specify the turbulent kinetic energy, and an algebraic equation is used to determine the length scale.

In addition to the geometry and thermal boundary conditions, there are two major governing parameters, the main flow Reynolds number, $Re = \rho UD/\mu$, and the rotational Reynolds number, $Re_\Omega = \rho\Omega D^2/\mu$. The Reynolds number ($Re$) represents the forced convection effect, and the rotational Reynolds number ($Re_\Omega$) reflects the cross-stream Coriolis effect. In the above equations, $\rho$ and $\mu$ are the density and viscosity of the air, $\Omega$ is the rotational speed.

The heat transfer performance is characterized by Nusselt number, which is defined as

$$Nu = hD/k = Dq_{\text{net}}/[k_{\text{air}}(T_w - T_b)] \qquad (1)$$

The notation $k_{\text{air}}$ stands for the thermal conductivity of the air, $T_w$ and $T_b$ are wall and air bulk temperatures, and $q_{\text{net}}$ is the net wall heat flux.

### Boundary Conditions

The inlet flow is of uniform velocity, uniform temperature (305.15 K), turbulent intensity 0.05, eddy length scale 0.002 m, and pressure of 1 atm (101,300 Pa). At the outlet, diminishing axial gradients of the variables are used. As to the four duct walls, two kinds of thermal boundary conditions are examined: (a) constant heat flux (CHF) without wall conduction, and (b) constant heat source applied but with heat loss through wall-conduction (CHS-WC).

In the latter conjugate heat transfer case (CHS-WC), heat loss through the outer surface of the model is considered. In the experiment, heating power is added to the heater. Most energy is transferred to the coolant air whose temperature is increased through the channel. Some heat energy is conducted through the fiberglass and escaped to the surroundings. The heat loss ($Q_L$) can be calculated by $Q_L = hA(T_{\text{wf}} - T_{\text{sur}})$, here $h$ denotes the convection heat loss coefficient, $T_{\text{sur}}$ the ambient temperature, $A$ the heat transfer (loss) area, and $T_{\text{wf}}$ is the wall temperature on the outer surface of the fiberglass.

The heat loss coefficients at four surfaces are evaluated separately by using conventional heat transfer correlation from textbooks, *e.g.*, Incropera and DeWitt (1996). At stationary condition, the heat losses from the four outer surfaces of the model are estimated by natural convection correlation of a heated plate. For rotating case, the

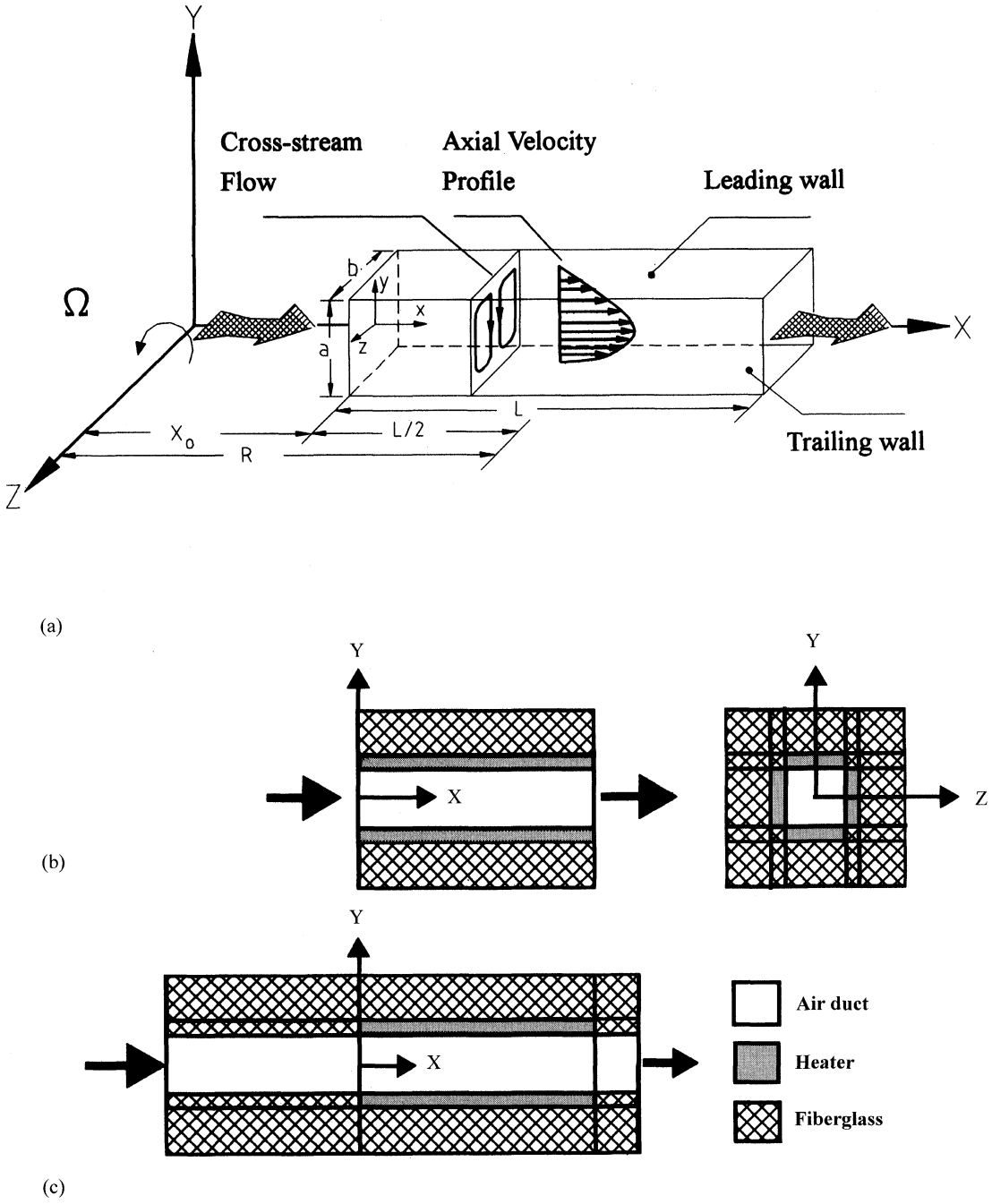


FIGURE 1 Physical model and coordinate system: (a) flow channel and coordinates; (b) sectional views of model without channel extension; (c) sectional views of model with channel extensions.

heat losses from the leading and trailing walls are calculated by using the stagnation and base flow heat transfer coefficients, while that from two side-walls by forced convection over flat plate. The local velocity at each radial location is used to determine the local Reynolds number and, then,

the local heat loss coefficient can be evaluated from the proper empirical formulas.

## METHOD OF SOLUTION

The present study employs a commercial software package "CFX-TASCflow" from AEA Technology (1998) to solve the three-dimensional Reynolds-averaged Navier–Stokes and energy equations. The transport equations are discretized by using a conservative finite-volume method. A collocated variable approach solves for the primitive variables in either stationary or rotating coordinate systems. A second-order skew upwind difference scheme with physical advection correction is used to solve the discretized linear algebraic equations. Two-layer turbulence model is used in the computations.

### Grid Systems

To find appropriate grid distribution, grid independence test at Reynolds number 10000 and outlet to inlet bulk temperature difference, $T_{b,e}-T_i=30\,\mathrm{K}$ under stationary and rotational conditions with rotational Reynolds number 162.2 for the CHF and CHS-WC cases are examined. For the CHF cases, evenly-spaced (*i.e.*, grid ratio $r_x=1.0$) grid distribution of 31 points in $X$ direction with seven non-uniform variations ($r_y=r_z=1.5$): (1) $21\times21$, (2) $25\times25$, (3) $29\times29$, (4) $33\times33$, (5) $37\times37$, (6) $41\times41$ and (7) $45\times45$ in $Y\times Z$ planes are considered. The difference between $31\times29\times29$ and $31\times45\times45$ is less than 0.51%. Tests with $29\times29$ non-uniform grid in $Y\times Z$ planes, four uniform grid ($r_x=1.0$) of 31, 61, 121 and 241 in $X$ direction are performed and the difference between 31 and 241 is less than 1.53%. In the case of CHS-WC, it is found that the temperature solution for the solid wall is not sensitive to the grid. Arrangement of four grid divisions for each wall is reasonable. With channel extensions at two ends, more grid points are placed in axial direction.

In summary, two kinds of orthogonal grid system for the present computations are addressed as follow:

(a) At CHF condition, computations are preformed on $31\times29\times29$ (26071 nodes) grids in the inner air duct. There are 31 uniform grid points from inlet to exit in $X$ direction. The number of grid points in $Y$ and $Z$ directions is 29 with grid ratio of 1.5.
(b) At CHS-WC condition, computations are preformed on $31\times37\times37$ (42439 nodes) grids for the model without duct extension and $66\times37\times37$ (90354 nodes) grids for the model with duct extensions. The arrangement of the grids in the inner air duct is the same as that for CHF case. Solid walls are made of stainless steel heater and fiberglass. The present study uses one division for heater and three uniform divisions for fiberglass in the normal direction.

## RESULTS AND DISCUSSION

In the present study, simulation covers the parameter ranges of Reynolds number $Re=8200$, 10000 and 15500 and $Re_\Omega=0$, 53.4, 162.2 and 320.4 for both CHF and CHS-WC cases. In order to obtain the baseline, simulations under the stationary condition are first conducted. Then rotational conditions are performed. In the present study, $Nu_o$ and $Nu_\Omega$ stands for the Nusselt numbers at stationary and rotational conditions, respectively.

### Flow Pattern and Temperature Distribution

#### *Rotational Effects on Flow Pattern and Temperature Contours*

To examine flow pattern and temperature distribution in a radially rotating channel with wall conduction, Figure 2 shows the cross-sectional views at different rotational conditions but the same axial location $X/D=15$ of a typical

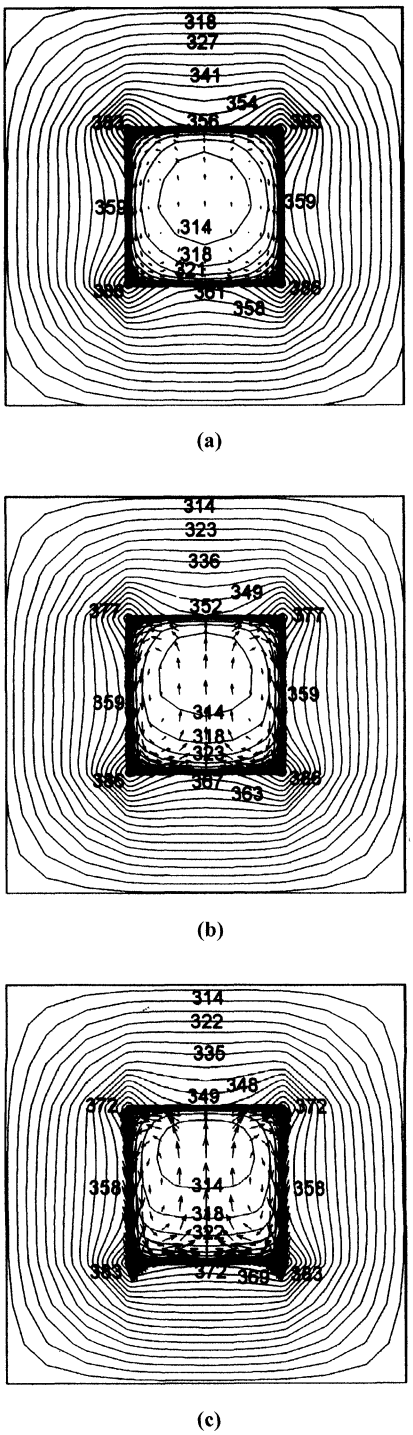


FIGURE 2 Flow patterns and temperature contours of CHS-WC case with channel extensions at $Re = 10{,}000$ and $X/D = 15$ under various rotational conditions: (a) $Re_\Omega = 53.4$; (b) $Re_\Omega = 162.2$; (c) $Re_\Omega = 320.4$.

CHS-WC case with channel extension at $Re = 10{,}000$. It is observed that, at $Re_\Omega = 53.4$, the Corolis-induced secondary flow is weak and the distortion or asymmetry of the isotherms is only a little. With $Re_\Omega$ raised up to 162.2 and 320.4, the rotational effect and, in turn, the secondary vortices become increasingly strong. Consider the flow in a stationary square channel, the field properties are symmetric with respect to both $Y$- and $Z$-axes. With the presence of the secondary flow under rotational condition, however, the isothermal lines cluster closely near the trailing wall. On the contrary, the isothermal lines near the leading wall appear sparse. It is also noted that the qualitative nature of the temperature distribution in the solid wall is not sensitive to the change in operating conditions. Therefore, in the following presentation, only the close-up views of the flow part are displayed for clarity.

### *Effects of Wall Conduction and Channel Extension*

Figures 3, 4, 5 and 6 depict axial evolution of the flow patterns and the temperature contours at various axial locations in the case of $Re = 10{,}000$ and $Re_\Omega = 162.2$. Results of CHF case without wall conduction and channel extension are shown in Figure 3. It is obvious that the strength of the secondary flow increases and the distortion of the isotherms becomes increasingly severe along the axial direction. Adding the channel extensions to the model, the thermal flow patterns change to those appearing in Figure 4. The computation is carried out on a model with unheated channel extensions at the two ends just like that used in the experiment. Under this condition, before the coolant airflow enters the heated channel, the flow in the extended part ($X/D < 0$) has been influenced by the rotational effects. Comparing the flow patterns on the plane of $X/D = 5$ in Figures 3 and 4, it is seen that the Coriolis-induced secondary vortices in Figure 4 are stronger than that in channel without extended part. At farther downstream part of the channel, *e.g.*, $X/D = 25$, the flow

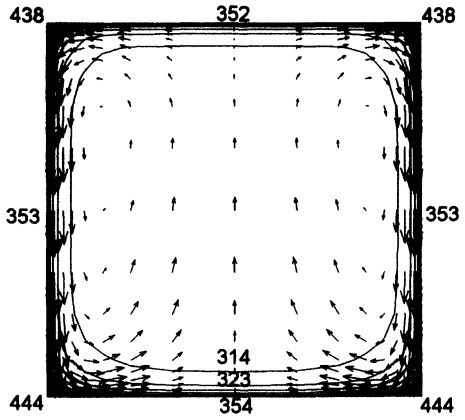


(a)

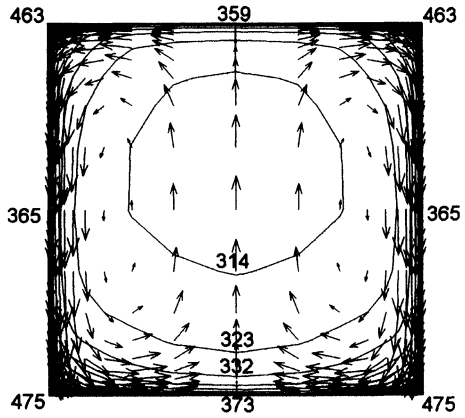


(b)

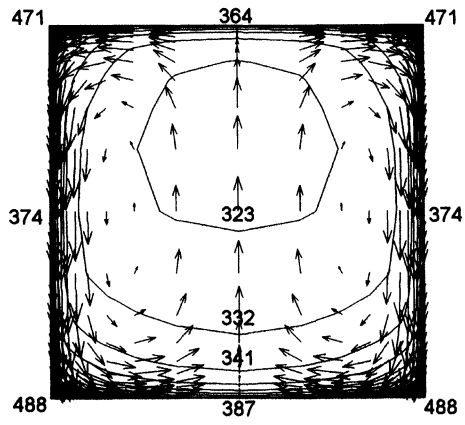


(c)

FIGURE 3 Flow patterns and temperature contours of CHF case without wall conduction and channel extensions at $Re = 10{,}000$ and $Re_\Omega = 162.2$: (a) $X/D = 5$; (b) $X/D = 15$; (c) $X/D = 25$.

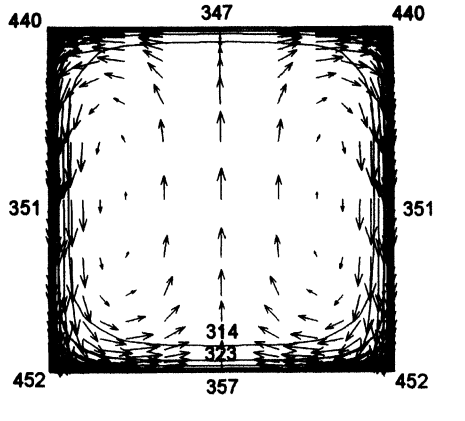


(a)

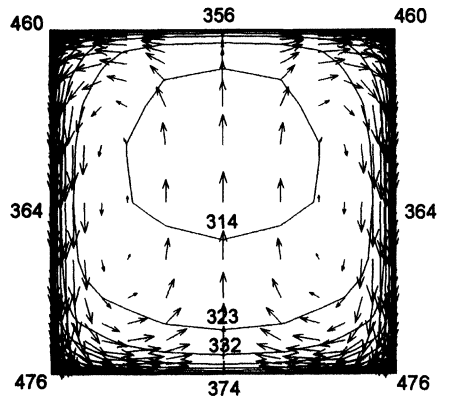


(b)

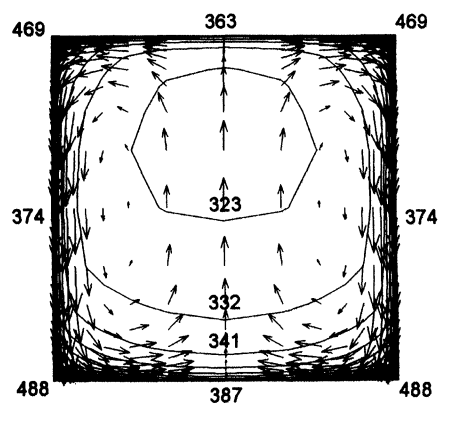


(c)

FIGURE 4 Flow patterns and temperature contours of CHF case without wall conduction but with channel extensions at $Re = 10{,}000$ and $Re_\Omega = 162.2$: (a) $X/D = 5$; (b) $X/D = 15$; (c) $X/D = 25$.

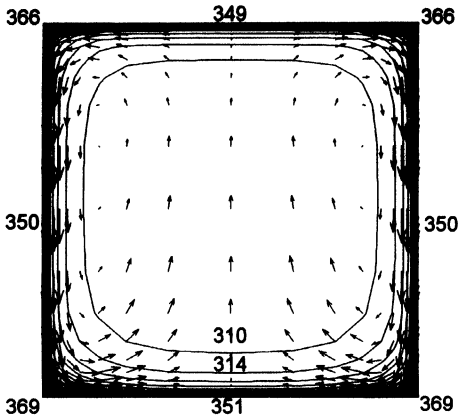


(a)

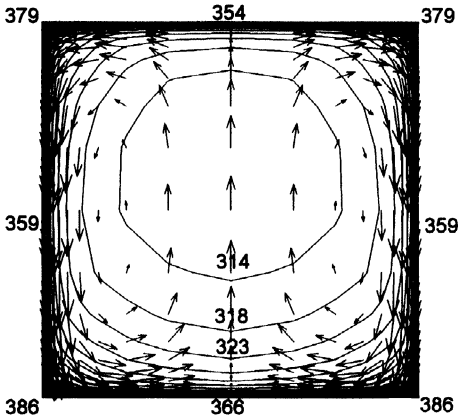


(b)

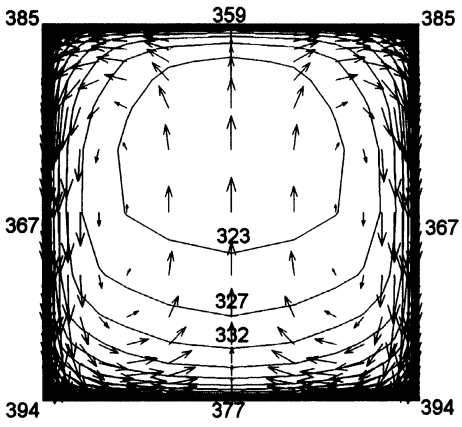


(c)

FIGURE 5 Flow patterns and temperature contours of CHS-WC case without channel extensions at $Re = 10{,}000$ and $Re_\Omega = 162.2$: (a) $X/D = 5$; (b) $X/D = 15$; (c) $X/D = 25$.

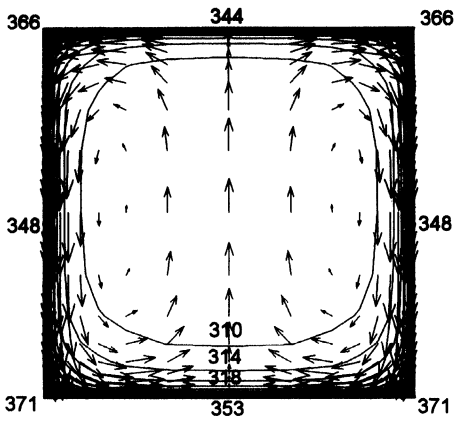


(a)

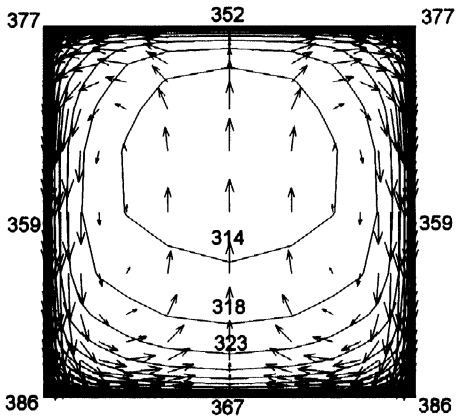


(b)

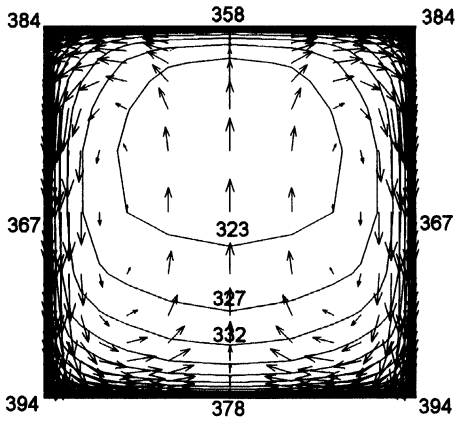


(c)

FIGURE 6 Flow patterns and temperature contours of CHS-WC case with channel extensions at $Re = 10{,}000$ and $Re_\Omega = 162.2$: (a) $X/D = 5$; (b) $X/D = 15$; (c) $X/D = 25$.

approaches fully developed and this superiority of strong secondary vortices diminishes gradually. With wall conduction included, Figures 5 and 6 show the same comparison of the secondary flow effects. Wall conduction and heat loss reduce the inner wall temperature noticeably, but comparisons of Figures 3 and 5 or 4 and 6 reveal that the wall conduction effect has little influence on the development of the secondary vortices in this low temperature and low speed flow. While the presence of the channel extension at the inlet end has only a little influence on the local wall and fluid temperatures.

### *Axial Temperature Distributions*

Since the measurements of the local velocity and temperature on a fast rotating model are quite difficult, there is a little detailed thermal-flow field data. Figures 7, 8 and 9 present comparisons of the present predictions for the typical cases mentioned above and the corresponding measurements of wall and fluid bulk temperatures in the Kuo and Hwang's work (1996). Both dimensional and dimensionless data are presented. In the three cases considered, all the predictions over-estimated the local wall and fluid temperatures. However, the present computations well catch the qualitative trend of the axial temperature variations. This point can be demonstrated by examining the temperature variation plotted in dimensionless form, *i.e.*, $\theta = (T_w - T_b)/(T_w - T_i)$, where $T_i$ is the inlet fluid temperature, and $T_w$ and $T_b$ denote local values of wall and fluid bulk temperatures, respectively. It is also noted that the computations for the case of CHS-WC show least deviations with the measurements.

## Heat Transfer Performance

### *Rotational Effects on Heat Transfer*

The rotational effect on the heat transfer is characterized by the ratio of Nusselt numbers in rotational to stationary cases, $Nu_\Omega/Nu_o$. The value

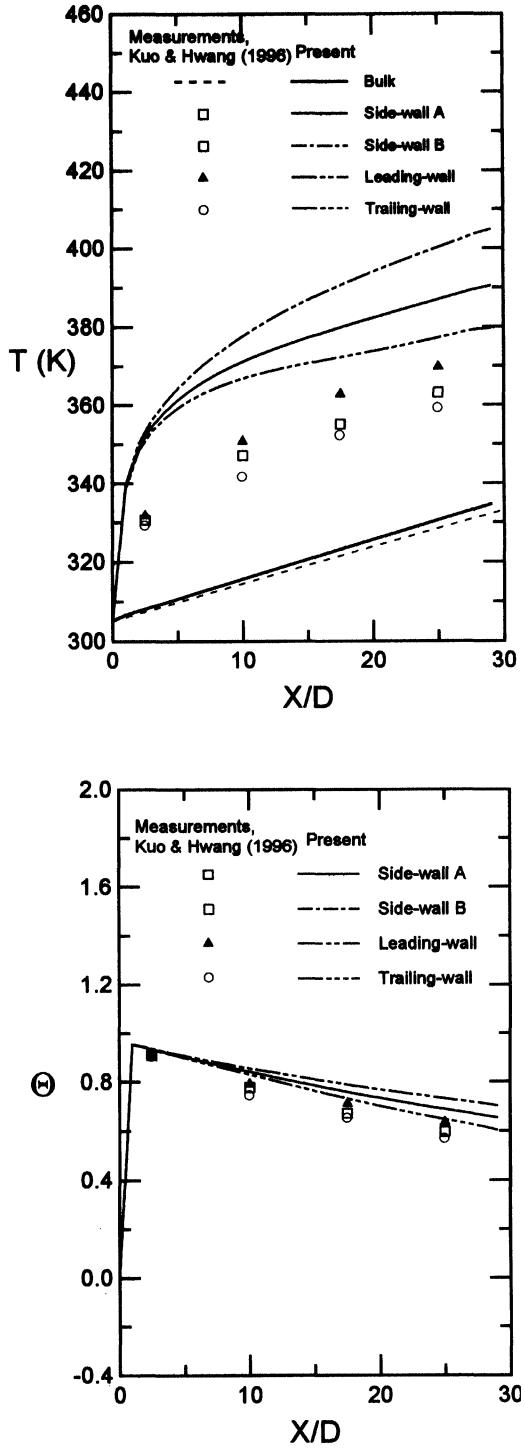


FIGURE 7 Dimensional and dimensionless axial temperature distributions of CHF case without channel extension at $Re = 10{,}000$ and $Re_\Omega = 162.2$.

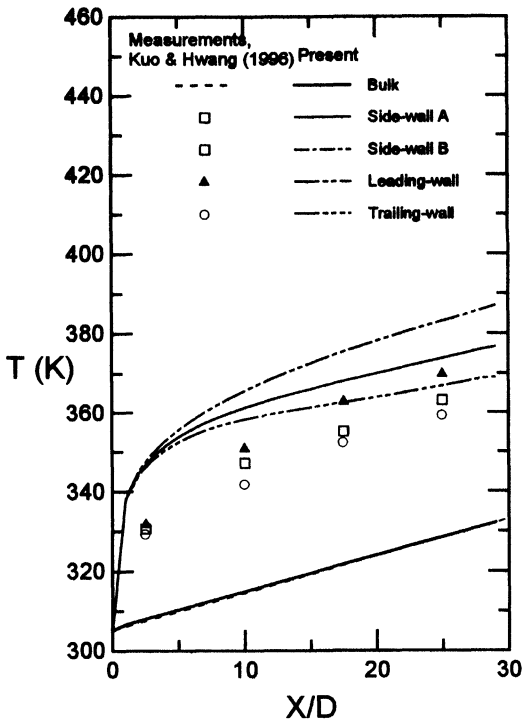


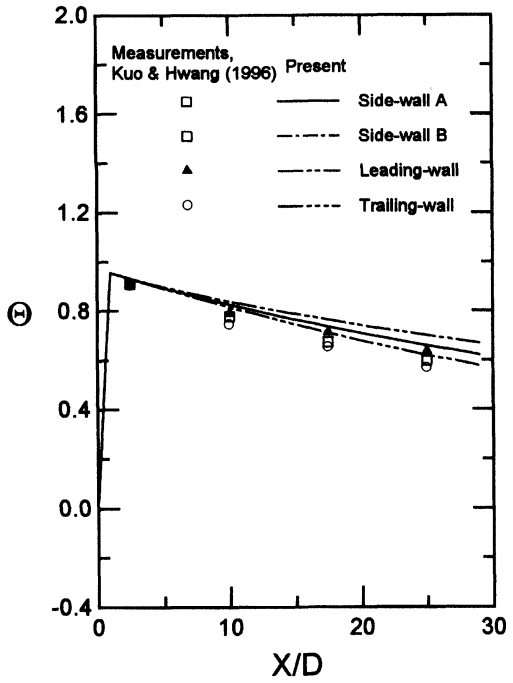


FIGURE 8 Dimensional and dimensionless axial temperature distributions of CHS-WC case without channel extension at $Re = 10{,}000$ and $Re_\Omega = 162.2$.

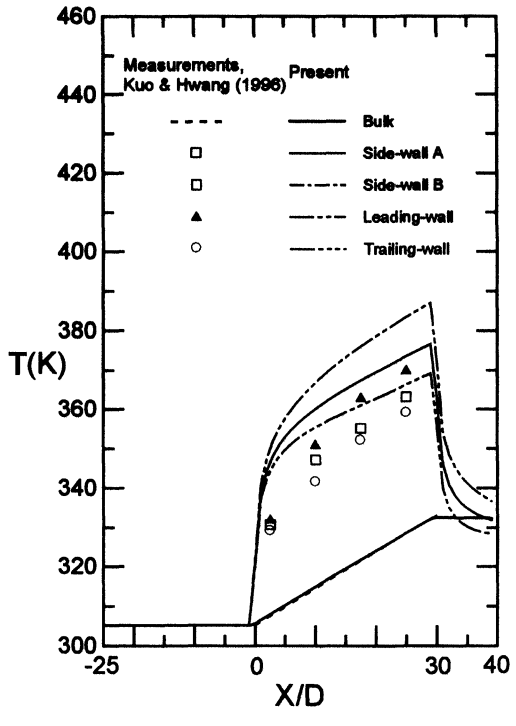


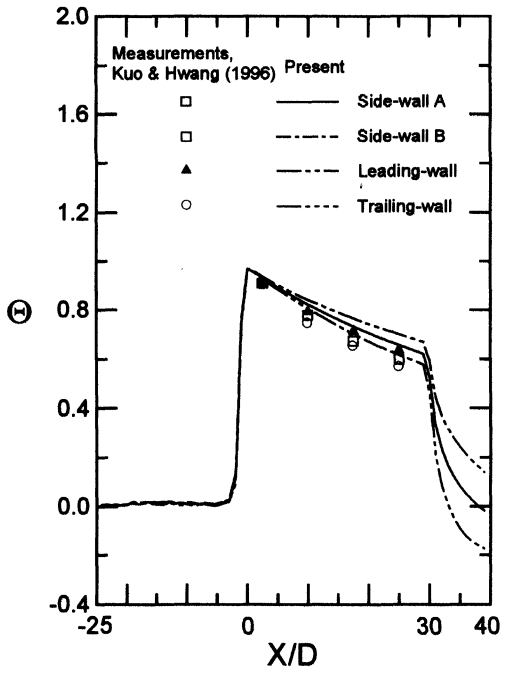


FIGURE 9 Dimensional and dimensionless axial temperature distributions of CHS-WC case with channel extensions at $Re = 10{,}000$ and $Re_\Omega = 162.2$.

of $Nu_\Omega/Nu_o > 1$ indicates the heat transfer enhancement, while $Nu_\Omega/Nu_o < 1$ indicates the heat transfer degradation by the rotational effect. The axial variations of $Nu_\Omega/Nu_o$ for the CHS-WC cases with channel extensions at $Re = 8200$, 10000 and 15500 and $Re_\Omega = 0$,53.4, 162.2 and 320.4 are shown in Figures 10, 11 and 12.

As shown in the Figures 10 to 12, the axial variation of $Nu_\Omega/Nu_o$ on the four walls of the channel are remarkably different. The major reason is the differences in the local thermal flow characteristics on four walls under the influences of Coriolis force. As the flow patterns and temperature contours shown in Figures 2–6, the Coriolis-induced cross-stream impinges directly on the trailing wall as the channel rotates. The secondary flow then carries the heated fluids away from the stagnation region, passes over the side-walls and towards the leading wall. Therefore this vortical motion creates additional mixing to the main flows and enhances the heat exchange between the fluids and the channel walls. The measured data show that the rotational effect on trailing wall is more pronounced than that on leading wall. This behavior is also well predicted by the present computations.

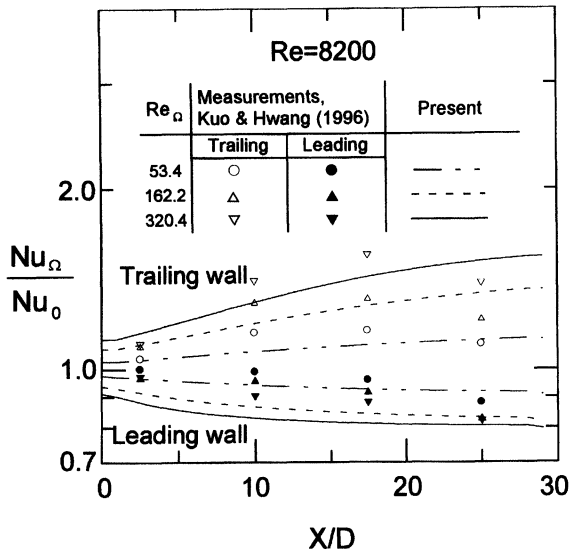


FIGURE 10 Axial variation of $Nu_\Omega/Nu_o$ on leading and trailing walls of CHS-WC model with channel extensions at $Re = 8200$.

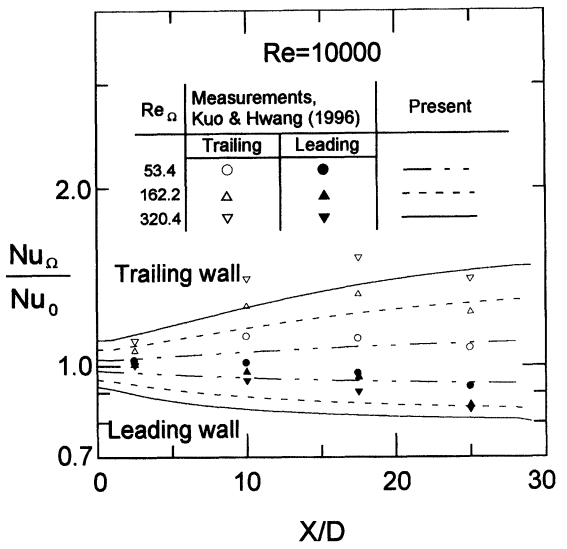


FIGURE 11 Axial variation of $Nu_\Omega/Nu_o$ on leading and trailing walls of CHS-WC model with channel extensions at $Re = 10000$.

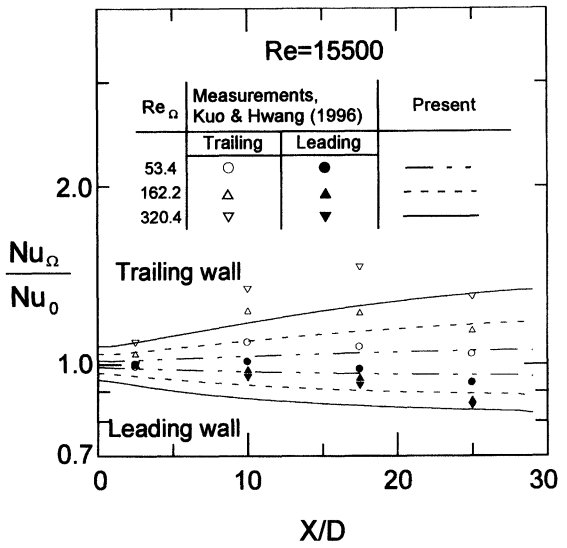


FIGURE 12 Axial variation of $Nu_\Omega/Nu_o$ on leading and trailing walls of CHS-WC model with channel extensions at $Re = 15500$.

### *Main Flow Reynolds Number Effects*

In Figures 10, 11 and 12, one can find that the Nusselt number ratio $Nu_\Omega/Nu_o$ reduces on both trailing and leading walls as $Re$ increases. Increasing $Re$

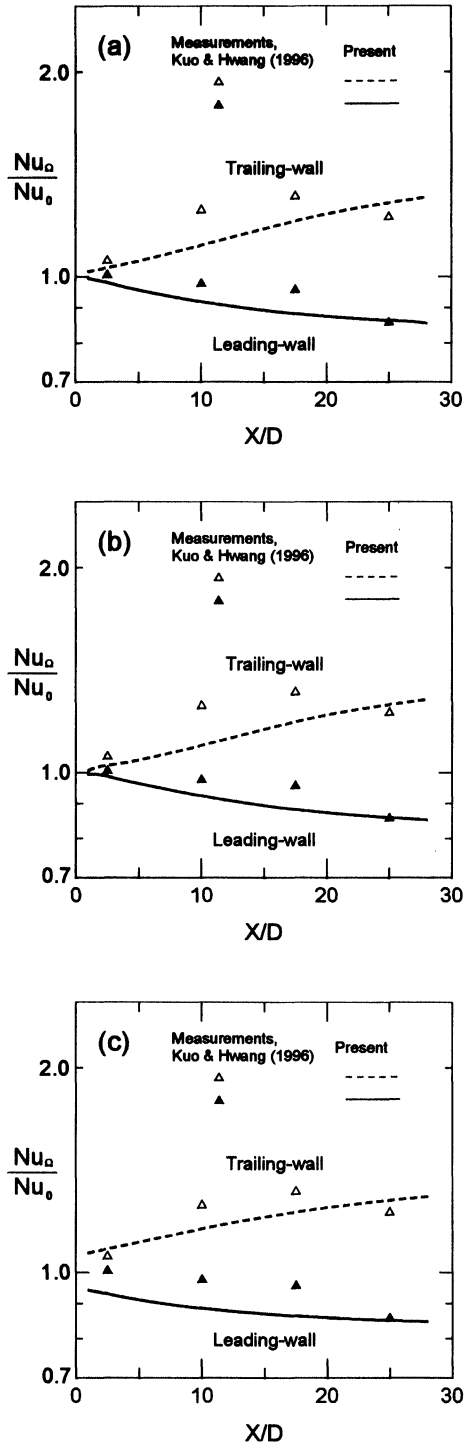


FIGURE 13 Comparison of $Nu_\Omega/Nu_o$ on leading and trailing walls of various models at $Re = 10{,}000$ and $Re_\Omega = 162.2$: (a) CHF model; (b) CFS-WC model without channel extension; (c) CHS-WC model with channel extensions.

strengthens the through flow and, relatively, the influence of the channel rotation becomes weaker.

### *Effects of Wall Conduction and Channel Extensions*

Figure 13(a) shows the results of CHF for the model without channel extensions. Figure 13(b) shows the results of CHS-WC for the model without channel extensions. Figure 13(c) shows the results of CHS-WC for the model with channel extensions. It is obvious that when the coolant air enters the channel, the local Nusselt numbers increase on trailing wall and decreases on leading wall under the influence of the rotation. The enhancement/degradation becomes severe for the growth of the Coriolis-induced secondary vortices along the axial direction. The above phenomena are also distinguished as the rotating rate increases. Although the present predictions deviate a little from the measured data of Kuo and Hwang (1996) in quantitative sense, the trends in *Nu* variations on either leading and trailing walls are well captured by the simulation.

In the real experiments, the wall conduction effect and the heat loss always exist. The heater and fiberglass walls have different thickness and different thermal conductivity. Through the wall conduction effects, the walls dissipate energy to the surroundings and, as comparison of the corresponding cases in Figures 13(a) and 13(b), the calculated heat transfer rates are lower than the results without wall conduction and heat loss.

The effects of the channel extensions can be addressed by comparing the corresponding cases in Figures 13(b) and 13(c). Basically, the effect of the channel outlet extension on heat transfer is small. Whereas the presence of the extended channel at the inlet modifies the local values of $Nu_\Omega/Nu_o$.

## CONCLUSIONS

The present paper presents a numerical study of turbulent heat transfer in a radially rotating square channel. The computations with two-layer

turbulence model have been performed at the conditions of Reynolds number $Re = 8200$, 10000 and 15500 and rotational Reynolds number $Re_\Omega = 0$, 53.4, 162.2 and 320.4 with/without consideration of wall conduction and channel extensions. Based on the present numerical results for this complex rotating flow configurations, the following conclusions can be drawn.

(1) Thermal flow characteristics in a radially rotating channel are strongly influenced by the Coriolis-induced secondary vortices. The secondary flow enhances heat transfer on trailing wall but degrades that on leading wall.
(2) Heat transfer ratio decreases on both trailing and leading walls with the increase in Reynolds number. Since the rotational effects becomes relatively weaker under the stronger forced flow condition. The ratio $Nu_\Omega/Nu_o$ demonstrated that the rotational effects on the trailing wall are more pronounced, and the situation becomes more obvious as the rotating rate or the rotational Reynolds number increases. Both the present computations and the previous measurements show the same trends.
(3) The present computational results reveal that the rotation-induced heat transfer enhancement on the CHS-WC model are lower than that on the CHF model, which is attributed to the presence of the wall conduction effect. The heat loss due to the wall conduction effect results in decreases in the inner wall temperature as well as the fluid bulk temperature.
(4) The channel extension has only a little influence on the local wall and fluid temperatures. However, with the presence of an upstream extension attached at the inlet of the heated channel, the secondary flow in the channel is strengthened due to the premature development of the Coriolis effect in the channel extension. In turn, the rotational effects on the local heat transfer can be enhanced especially in the inlet region of the channel.
(5) The present predictions depict major trend of the turbulent convection flow and heat transfer in a rotating channel and, quantitatively, the results are also reasonable. As to the deviation between the predictions and the measured data, the reasons are threefold. Firstly, since Kuo's heat transfer data were calculated based on the uniform heat flux (total heat input minus total loss), which is different from our Nusselt numbers based on the local values of net heat flux with the consideration of the local heat loss effect. It is believed that the latter data reduction is more reasonable. Unfortunately, we lack of the record of the detailed local heat loss in Kuo's experiments. In the present work, the heat loss was estimated by the conventional heat transfer correlation. Secondly, rotation-induced buoyancy effect is not included in the present computations. Since the centrifugal buoyancy may enhance heat transfer in a turbulent flow, it is expected that the computational model with consideration of density variation would generate better results. Finally, more appropriate turbulence model is needed for this complex flow including rotational and thermal effects.

***Acknowledgments***

The authors would like to thank MIRL, ITRI for the financial support of this work and Dr. C. R. Kuo of CAST, ITRI for his kindness in providing some of his measured data.

## NOMENCLATURE

| | |
|---|---|
| $A$ | heat transfer area, $m^2$ |
| $D$ | hydraulic diameter, m |
| $h$ | heat transfer coefficient, $W/(m^2 \cdot K)$ |
| $k$ | turbulent kinetic energy, J/kg |
| $k_{air}$ | thermal conductivity of air, $W/(m \cdot K)$ |
| $Nu$ | Nusselt number $= hD/k_{air} = Dq_{net}/[k_{air}(T_w - T_b)]$ |
| $Nu_o$ | Nusselt number for non-rotating condition |
| $Nu_\Omega$ | Nusselt number for rotating condition |
| $Q_L$ | total heat loss, W |

| | |
|---|---|
| $q_{net}$ | net wall heat flux, W/m$^2$ |
| $Re$ | through-flow Reynolds number = $\rho UD/\mu$ |
| $Re_\Omega$ | Rotational Reynolds number = $\rho\Omega D^2/\mu$ |
| $r_x$, $r_y$, $r_z$ | grid ratios in $X$-, $Y$- and $Z$-directions |
| $T_b$ | local coolant bulk temperature, K |
| $T_{b,e}$ | exit coolant bulk temperature, K |
| $T_i$ | inlet coolant bulk temperature, K |
| $T_{sur}$ | surrounding temperature, K |
| $T_w$ | local wall temperature, K |
| $T_{wf}$ | fiberglass wall temperature, K |
| $U$, $V$, $W$ | velocity component, m/s |
| $X$, $Y$, $Z$ | distance along main flow direction for all passages, m |

*Greek Symbols*

| | |
|---|---|
| $\varepsilon$ | turbulence dissipation rate, W/kg |
| $\mu$ | dynamic viscosity, m$^2$/s |
| $\rho$ | coolant air density, kg/m$^3$ |
| $\theta$ | $(T_w - T_b)/(T_w - T_i)$ |
| $\Omega$ | rotation rate, rad/s |

## References


Abdelmeguid, A. M. and Spalding, D. B. (1979) Turbulent flow and heat transfer in pipes with buoyancy effects, *Journal of Fluid Mechanics*, **94**, 383–400.

Dutta, S., Andrews, M. J. and Han, J. C. (1996) Prediction of turbulent heat transfer in rotating smooth square ducts, *International Journal of Heat and Mass Transfer*, **19**, 2505–2514.

Han, J. C. and Zhang, Y. (1992) Effect of uneven wall temperature on local heat transfer in a rotating square channel with smooth walls and radial outward flow, *ASME Journal of Heat Transfer*, **114**, 850–858.

Hwang, G. J., Tzeng, S. C. and Mao, C. P. (1999) Heat transfer of compressed air flow in a spanwise rotating four-pass serpentine channel, *ASME Journal of Heat Transfer*, **121**, 583–591.

Iacovides, H. and Launder, B. E. (1987) Turbulent Momentum and Heat Transport in Square-Sectioned Duct Rotating in Orthogonal Mode, *Numerical Heat Transfer*, **12**, 475–491.

Iacovides, H. and Launder, B. E. (1991) Parametric and numerical study of fully developed flow and heat transfer in rotating rectangular duct, *ASME Journal of Turbomachinery*, **113**, 331–338.

Iacovides, H. and Launder, B. E. (1995) Computational fluid dynamics applied to internal gas-turbine blade cooling: A review, *International Journal of Heat and Fluid Flow*, **16**, 454–470.

Incropera, F. P. and DeWitt, D. P. (1996) *Introduction to Heat Transfer*, Third edn., John Wiley & Sons, New York, USA.

Johnston, J. P., Halleen, R. M. and Lezius, D. K. (1972) Effects of spanwise rotation on the structure of two-dimensional fully developed turbulent channel flow, *Journal of Fluid Mechanics*, **56**, 533–557.

Kuo, C. R. and Hwang, G. J. (1996) Experimental studies and correlations of radially outward and inward air-flow heat transfer in a rotating square duct, *ASME Journal of Heat Transfer*, **118**, 23–30.

Morris, W. D. and Ghavami-Nasr, G. (1991) Heat transfer measurements in rectangular channels with orthogonal mode rotation, *ASME Journal of Turbomachinery*, **113**, 339–345.

Soong, C. Y., Lin, S. T. and Hwang, G. J. (1991) An experimental study of convective heat transfer in radially rotating rectangular ducts, *ASME Journal of Heat Transfer*, **113**, 604–611.

Wagner, J. H., Johnson, B. V. and Kopper, F. C. (1991) Heat transfer in rotating serpentine passages with smooth walls, *ASME Journal of Turbomachinery*, **113**, 321–330.

AEA Technology (1998) CFX-TASCflow user documentation, AEA Technology Engineering Software Ltd., UK.